

## THE FLOW PAST PARTICLES DRIVEN BY A PRESSURE GRADIENT IN SMALL TUBES

Gregory J SHEARD<sup>1</sup> and Kris RYAN<sup>1</sup>

<sup>1</sup> Fluids Laboratory for Aeronautical and Industrial Research (FLAIR), Department of Mechanical Engineering, Monash University, VIC 3800, AUSTRALIA

### ABSTRACT

The flow past a series of spheres moving through a tube is computed using axisymmetric and three-dimensional spectral-element methods. For a specific ratio of sphere to tube diameter, and sphere spacing, critical Reynolds numbers for conditions of both zero flow relative to the spheres, and zero net axial forces on the spheres are established. An axisymmetric Hopf transition to unsteady flow is identified, and Landau modelling characterizes the instability as occurring through a supercritical bifurcation. The variation in key flow parameters with changes in diameter ratio and sphere spacing are also established.

### NOMENCLATURE

DR	diameter ratio
SR	sphere spacing ratio
$Re$	Reynolds number
$V$	sphere velocity
$D$	tube diameter
$d$	sphere diameter
$S$	distance between spheres
$\nu$	kinematic viscosity
$Q$	flow rate
$Q_{rel}$	flow rate relative to spheres
$P$	kinematic pressure
$dP/dz$	axial kinematic pressure gradient
$F_D$	drag force acting on each sphere
$\mathbf{u}$	velocity vector
$u_z, u_r$	axial and radial velocity components
$u_x, u_y, u_z$	Cartesian velocity components

### INTRODUCTION

Owing to the myriad practical applications of the fundamental problem of fluid flowing in a tube containing suspended solid bodies, there has been an extensive history of analytical (Smythe, 1961 & 1964; Lighthill, 1968; Fitz-Gerald, 1969), and more recently numerical (Tözeren & Skalak, 1978 & 1979; Wang & Parker, 1998; Ortega, Bristol & Savas, 1998; Secomb, Hsu & Pries, 1998 & 2001) attempts to investigate these flows systems. The primary motivation for this study is driven by an interest in bio-fluid dynamics as it pertains to blood flow in narrow vessels such as arterioles, where the scale of red blood cells is of the same order as the vessel calibre (inner diameter). Other engineering applications also exist, though, including the passage of colloidal solutions through narrow orifices and tubes, the flushing of obstructions from pipes, and annular flows around obstacles.

The earliest theoretical attempts to tackle the problem of the flow past a body in a tube were performed by Smythe

(1961; 1964), who first developed and subsequently revised an analytical solution for the potential flow past a single sphere in an infinitely long tube, expressing the result as an effective increase in tube length caused by the increased pressure drop past the obstruction.

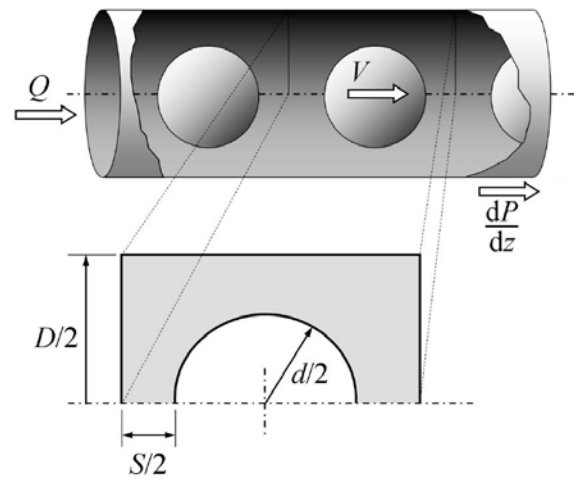


Figure 1: Schematic diagram of the system.

Lighthill (1968) derived a model incorporating a viscous lubricating layer between body and tube wall for the flow past deformable axisymmetric pellets driven by a pressure gradient through an elastic tube. He predicted necking behind the body similar in appearance to a peristaltic driving force, which suggested the potential for misinterpretation of experimental observations of such flows. The work of Lighthill was extended by Fitz-Gerald (1969), who considered the deformation of red blood cells in the type of flow investigated by Lighthill. A significant finding from that study was the prediction that in vessels with calibres in the range 5-7  $\mu\text{m}$ , resistances up to 7 times higher than predicted using Poiseuille's Law and the viscosity of whole blood (including plasma, red blood cells, and other components).

The work of Tözeren & Skalak (1978; 1979) was the first to study a series of bodies rather than a single body in a tube, and again axisymmetry in motion was assumed. Important in these studies was the demonstration that the zero-net-drag condition, corresponding to the condition at which a body would maintain constant velocity in a tube, was predicted with greater accuracy than by the model of Fitz-Gerald (1969). Beyond the scope of the present study, Tözeren (1983) also investigated the non-axisymmetric motion of bodies in a tube. Pozrikidis (2005) gave numerical evidence suggesting that spherical

bodies tended to migrate towards the tube centreline, supporting the validity of the axisymmetric assumption of the present study. In Ortega *et al.* (1998) evidence was found that useful data on flow resistance past multiple spheres could be obtained without resorting to the expensive task of modelling body and tube compliance, and possibly even body compressibility.

Important contributions to the understanding of the motion of red blood cells small through vessels were made by Secomb *et al.* (1998; 2001). They used a numerical model incorporating effects such as the presence of an endothelial surface layer and the elasticity of the cell membrane to accurately reproduce the deformed cell shapes observed experimentally.

The present study seeks to investigate the fundamental problem of pressure-driven flow past an equi-spaced series of axisymmetrically positioned spheres moving through a tube. Thus with variation in a Reynolds number

$$Re = \frac{VD}{\nu},$$

based on the tube diameter ( $D$ ), sphere velocity ( $V$ ) and fluid kinematic viscosity ( $\nu$ ), geometric parameters including a diameter ratio

$$DR = d/D,$$

based on the sphere diameter ( $d$ ) and the tube diameter, a spacing ratio

$$SR = S/d,$$

incorporating the sphere spacing ( $S$ ), and also the imposed axial pressure gradient  $dP/dz$ , a rich parameter space is available for investigation.

A schematic representation of the system under investigation is provided in figure 1. As well as the quantities defined previously, this figure also includes the fluid flow rate,  $Q$ , through the tube.

## NUMERICAL METHODOLOGY

In this study both axisymmetric and three-dimensional spectral-element computations are performed. The axisymmetric computations are performed on a two-dimensional mesh of nodal quadrilateral spectral elements occupying the meridional half-plane of the computational domain in cylindrical coordinates (i.e., mesh occupies the  $z$ — $r$  plane, and zero gradients in the azimuthal  $\theta$  direction are enforced). The three-dimensional computations are performed on a mesh of nodal hexahedral spectral elements encompassing the computational domain. Three-dimensional computations are performed in Cartesian coordinates.

In vector form, the incompressible Navier—Stokes equations can be written

$$\frac{\partial \mathbf{u}}{\partial t} + \mathbf{u} \cdot \nabla \mathbf{u} = -\nabla P + \nu \nabla^2 \mathbf{u},$$

$$\nabla \cdot \mathbf{u} = 0,$$

where  $\mathbf{u}$  is the velocity vector,  $P$  is the kinematic static pressure, and  $\nu$  is the kinematic viscosity. The axisymmetric form of the vector operators can be found in Blackburn & Sherwin (2004), and the three-dimensional form is given in Karniadakis & Sherwin (2005).

Both the axisymmetric and three-dimensional formulations are implemented through the in-house spectral-element software package *Viper* developed by

author G.J.S. The software exclusively employs a nodal-based spectral-element formulation (Karniadakis & Sherwin, 2005) with Gauss—Legendre—Lobatto quadrature used to integrate the weak form of the equations over each element.

## Boundary conditions

In this study periodic velocity boundary conditions are employed in the axial direction to efficiently simulate an infinite series of equi-spaced spheres moving through a tube. To drive the flow past the spheres, unequal Dirichlet conditions were prescribed on each of the periodic velocity boundaries. This constraint was based on the assumption that no radial variation in pressure exists at the mid-plane between each pair of spheres. Studies employing meshes which included multiple spheres have verified that this constraint provides errors in flow rate and forces on the spheres of less than 2% for Reynolds numbers  $Re < 200$ . On the axis, zero radial velocity and pressure gradients are enforced, on the tube wall a Dirichlet velocity condition  $u_z = -V$  is imposed to correctly describe the moving sphere condition, and on the surface of the sphere, zero velocity is enforced.

Time integration is performed using a three-step splitting scheme based on a backwards-multistep formulation (Karniadakis, Israeli & Orszag, 1991; Blackburn & Sherwin, 2004), with an appropriate high-order Neumann boundary condition for pressure imposed where Dirichlet pressure values are not specified.

## Mesh and grid independence

The axisymmetric mesh employed for this study is shown in figure 2. For much of this study, the parameters investigated are  $SR = 1.0$  and  $DR = 0.6$ , which is reflected in this particular mesh. The concentration of elements towards the mesh boundaries was performed to either localize errors due to artificial boundaries (i.e., periodic boundaries), or to provide added resolution near regions of higher shear. Figure 2 reveals both the distribution of spectral elements, and the interpolation points within each element (here 6<sup>th</sup>-order elements are employed).

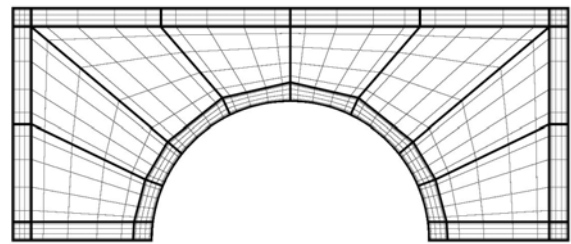


**Figure 2:** Mesh employed for axisymmetric computations. Thick lines denote spectral elements, and faint lines indicate location of elemental quadrature points.

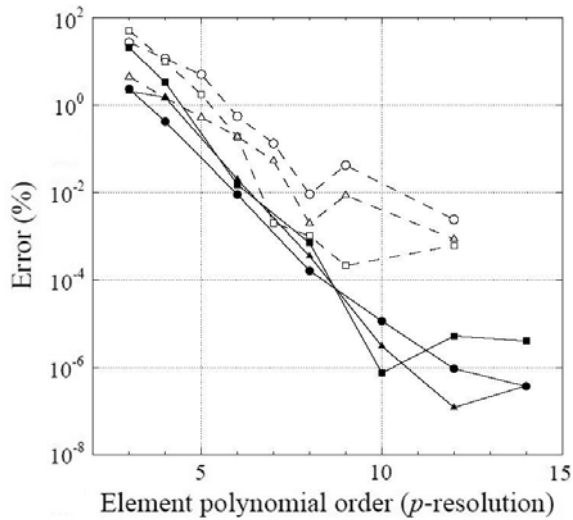


**Figure 3:** Convergence of flow quantities with increasing element order ( $p$ -resolution) for the axisymmetric mesh at Reynolds numbers  $Re = 1$  (solid lines and symbols) and  $Re = 100$  (dashed lines and open symbols). Circles, squares and triangles denote error in flowrate, pressure and viscous drag components, respectively.

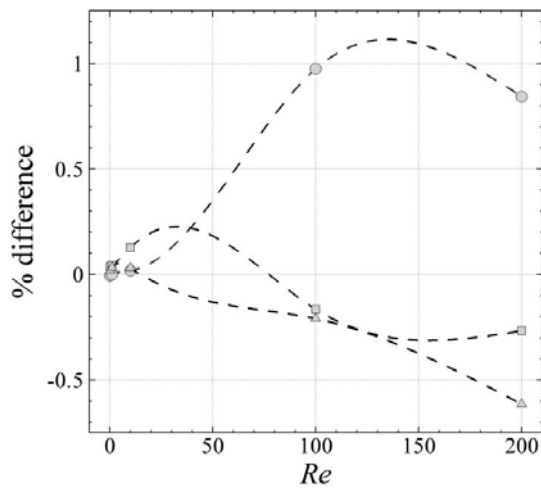


**Figure 4:** Percent differences as a function of Reynolds number between single-sphere and four-sphere computations. Dashed lines are added for guidance, and relative flow rate, and pressure and viscous axial force components are indicated by circles, squares and triangles, respectively.

For the chosen mesh, a grid-independence study was performed, with errors in the flow rate relative to the spheres, and the pressure and viscous contributions to the drag on the spheres being monitored for convergence with increasing element order ( $p$ -refinement). The results of this analysis are shown in figure 3, where trends showing near spectral convergence at moderate resolutions can be seen for Reynolds numbers  $Re = 1$  and  $Re = 100$ . The convergence is superior at  $Re = 1$ , indicating the validity of the periodic velocity/uniform pressure boundary condition on the boundaries on the axial extremes of the mesh.

To test the validity of the pressure-driven periodic boundary treatment further, comparative numerical tests

were performed on a mesh containing four successive spheres, rather than just the one. Therefore the artificial boundary was imposed between every fourth sphere, instead of between every sphere. Figure 4 shows a plot of the difference in flow quantities between single-sphere and four-sphere simulations, and as can be seen, the overall discrepancies remain below 1%, even up to  $Re = 200$ , validating the use of this type of boundary.

For three-dimensional computations, a hexahedral mesh was carefully constructed to incorporate a similar element distribution to the axisymmetric mesh. The plot in figure 5 shows a cutaway view, exposing the sphere surface, of the mesh employed for three-dimensional computations. Identical boundary conditions were imposed for three-dimensional computations, with the exception of the axis boundary condition, which was not required in the three-dimensional case.

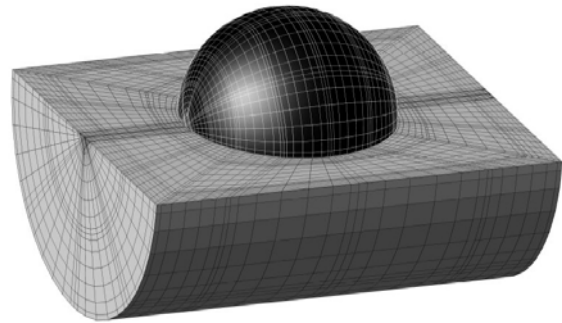


**Figure 5:** Cutaway of hexahedral mesh employed for three-dimensional computations. Only the lower half of the domain (shaded grey) is shown to reveal the boundary defining the sphere (shaded black).

#### Parameter space

While this study is motivated by low-Reynolds-number applications such as blood flow in narrow vessels, the goal is to explore the parameter space in terms of Reynolds number and pressure gradient in such a way that a description of the flow dynamics will be made for a wide range of parameters, ideally encompassing unsteady and three-dimensional flow transitions. Based on existing knowledge of similar transitions in sphere wakes, and the understanding that with an increase in blockage instabilities tend to occur at higher Reynolds numbers, it was decided that for a unit kinematic pressure drop across the computational tube unit, Reynolds numbers up to and including  $Re = 1000$  will be investigated.

Predominantly, geometric parameter values in the range  $SR = 1.0$  and  $DR = 0.6$  are employed, though this study also reports on variation of these values over the ranges  $0.2 \leq SR \leq 1.8$ , and  $0.1 \leq DR \leq 0.9$ .

## RESULTS

### Flow dynamics for a single geometry

For the reference system (with geometric parameters  $SR = 1.0$  and  $DR = 0.6$ , and a unit pressure drop across the repeating tube unit), the flow rate relative to the spheres ( $Q_{rel}$ ) was determined for a wide range of Reynolds numbers. Unsteady flow was identified above  $Re \approx 730$ , and for unsteady flows the envelope of the computed flow rates was monitored. A plot of the resulting data is shown in figure 6, which reveals notable features including a transition point between negative and positive flow

relative to each sphere which occurs at  $Re \approx 111.5$ . It can be seen that in the limit as  $Re \rightarrow 0$ , a minimum relative flow rate of  $Q_{rel} \approx -0.38$  is found. The gradient at Reynolds numbers less than  $Re \approx 200$  is highly linear, but at higher Reynolds numbers the slope becomes slightly shallower. Interestingly, beyond the transition to unsteady flow, an almost imperceptible oscillation in flow rates is recorded, with the maximum and minimum envelope lines almost coincident.

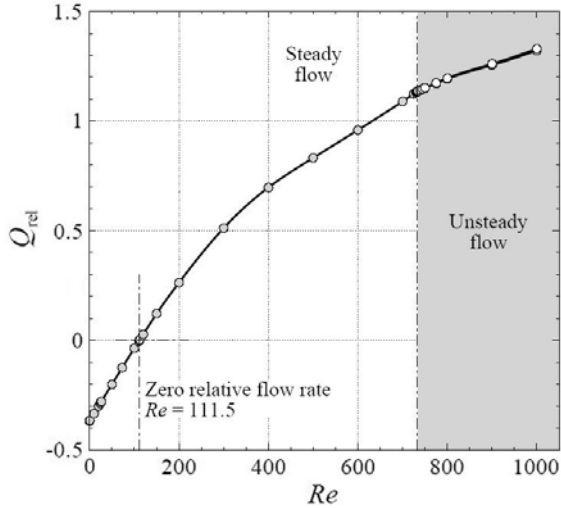


**Figure 6:** Flow rate relative to spheres ( $Q_{rel}$ ) plotted against Reynolds number for a geometric configuration with  $SR = 1.0$  and  $DR = 0.6$ . Unsteady flow was detected in the shaded region, and in this region lines through local minima and maxima in the time-varying flow rate is plotted.

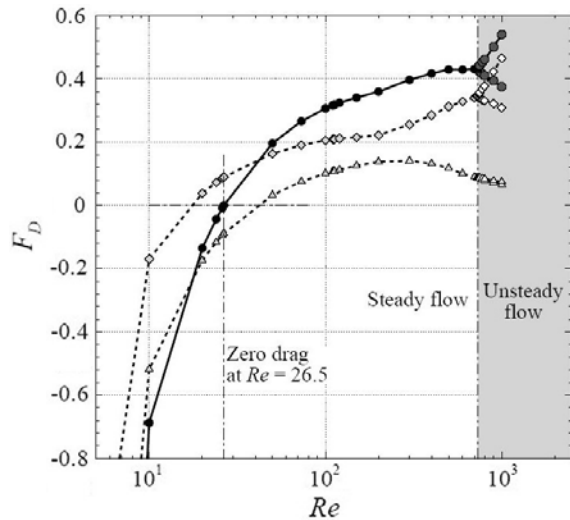


**Figure 7:** Total drag force (solid lines and “•”) and pressure and viscous (dotted lines and “◊” and “Δ”, respectively) contributions plotted against Reynolds number for a geometric configuration with  $SR = 1.0$  and  $DR = 0.6$ . Unsteady flow was detected in the shaded region, and in this region lines through local minima and maxima in the drag forces are plotted.  $F_D$  acts in the axial direction.

Important to the motion of spheres free to propagate in a pressure-driven flow is the axial force acting on each

sphere. If the spheres are exposed to a negative (or drag) force, they will decelerate, whereas the opposite is true if the net force acts in the direction of flow. The equilibrium position therefore requires that the net axial force is zero. Contributions to this axial force were computed from surface integrals of axial components of either pressure or shear stress on the sphere, and both the components and the total force are plotted for a range of Reynolds numbers in figure 7.

The axial force trends reveal that the zero net drag condition corresponding to the equilibrium position for freely suspended spheres occurs at  $Re \approx 26.5$ . At this point the pressure force is positive, and the viscous force is negative. This is in agreement with the relative flow rate trend in figure 6, which shows a negative flow rate relative to the spheres at the zero-net-drag condition. Despite only small variation in the viscous drag envelope beyond the transition to unsteady flow, a large oscillation in the pressure contribution emerges rapidly. Notice also that the force components all rapidly approach large negative values in the limit of low Reynolds numbers. This is in agreement with the theoretical analyses discussed earlier, where it was shown (e.g., Fitz-Gerald, 1969) that for physiologically realistic parameters that the presence of an obstruction greatly increased the resistance to flow.

Despite the lack of linearity in the low-Reynolds number trend as compared with the flow rate trend in figure 6, the axial force data can be found to achieve a linear collapse if the data is re-plotted as the product  $Re F_D$ . Further computations were performed over a range of both axial pressure gradients and Reynolds numbers, and it was determined that a successful collapse of the data could be obtained if it were plotted against the product  $Re dP/dz$ . These collapses are provided in figure 8, for both the relative flow rate and axial force data sets. In each case an excellent collapse is found for small  $Re dP/dz$  values, though the  $Q_{rel}$  data collapse is less successful beyond  $Re dP/dz \approx 1000$ .

#### Flow dynamics with geometry variation

The previous results were obtained with the geometric parameters fixed at  $SR = 1.0$  and  $DR = 0.6$ . A family of consistent meshes were generated to extend this study to geometric configurations occupying a range of diameter and spacing ratios. In this case it was necessary to prescribe unique pressure drops across each mesh as the length of the computational tube unit differed between each mesh. A constant pressure gradient of  $dP/dz = 0.8333$  was applied in each case, consistent with the pressure gradient resulting from the unit pressure drop imposed in the earlier computations. Simulations were performed on each mesh for a Reynolds number  $Re = 1$ , and a comparative set of contour plots was generated to compare the flows with variation in each parameter independently. Figure 9 shows the resulting plots, with the effect of changing either the diameter ratio or the spacing ratio denoted by each column. It is curious to observe that with variation in diameter ratio, there is a marked alteration in the vorticity distribution surrounding the sphere, whereas with variation in spacing, the vorticity distribution remains almost unchanged. This implies that at this Reynolds number, the alteration to the otherwise uniform flow through the tube is localized to a region very close to the sphere obstructing the flow. It follows, then,

that almost irrespective of the sphere spacing, each sphere will cause a consistent added pressure drop to the flow.

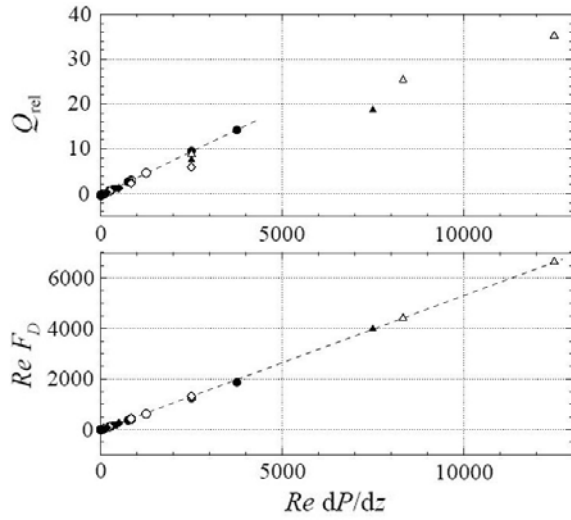


**Figure 8:** Plots showing collapse of the flow rate relative to the spheres ( $Q_{rel}$ ) and the product of the Reynolds number and the net axial force acting on each sphere ( $Re F_D$ ) when plotted against the product of the Reynolds number and pressure gradient  $Re dP/dz$ . Symbols “□”, “■”, “○”, “●”, “△”, “▲”, “◇” and “◆” represent  $Re = 0.1, 0.3, 1, 3, 10, 30, 100$  and  $200$ , respectively. The dotted lines are added for guidance to indicate the data which fits the universal collapse.

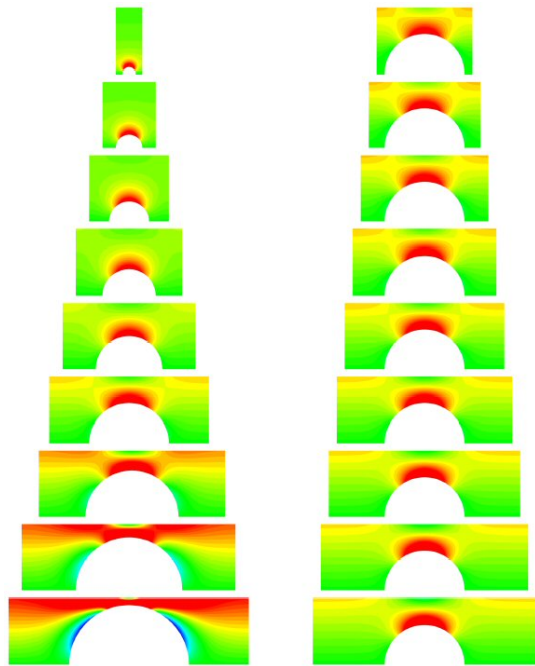


**Figure 9:** Contour plots of vorticity in the flow around spheres in tubes. Left: Diameter ratios (top to bottom)  $DR = 0.1, 0.2, 0.3, 0.4, 0.5, 0.6, 0.7, 0.8$  and  $0.9$  for a constant spacing  $SR = 1.0$ . Right: Spacing ratios (top to bottom)  $SR = 0.2, 0.4, 0.6, 0.8, 1.0, 1.2, 1.4, 1.6$  and  $1.8$  for a constant diameter ratio  $DR = 0.6$ . In all cases  $Re = 1$  and  $dP/dz = 0.8333$ . Blue and red regions correspond to negative and positive vorticity, respectively.

With increasing diameter ratio a large increase in the amount of vorticity surrounding the sphere is created. This effect becomes so pronounced that for  $DR > 0.5$  a large region of shear is generated along the tube wall, becoming stronger as the shear gradients in the fluid layer between the wall and the sphere become higher as the gap reduces.

### Non-axisymmetric flow transition

The axisymmetric computations reveal that a transition to an axisymmetric unsteady flow occurs at  $Re \approx 730$ . It is known, though, that for a single sphere in an otherwise undisturbed freestream, the axisymmetric wake bifurcates to a non-axisymmetric state through a regular (i.e., steady-state) transition at  $Re = 211$  (Ghidersa & Dušek, 2000; Thompson, Leweke & Provansal, 2001). This transition occurs far earlier than any theoretical transition of the axisymmetric wake to an unsteady state, and significantly earlier than the subsequent non-axisymmetric transition to unsteady flow found for spheres at  $Re = 275$  (Thompson, Leweke & Provansal, 2001; Sheard, Thompson & Hourigan, 2003).

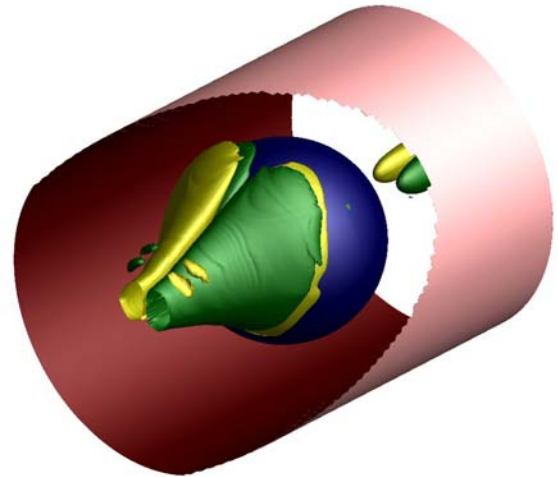


**Figure 10:** Iso-surface plot showing the structure of the non-axisymmetric flow at  $Re = 360$  with  $DR = 0.6$  and  $SR = 1.0$ , computed using the three-dimensional solver and mesh. Flow is from top right to bottom left, yellow and green contours reveal negative and positive regions of streamwise vorticity, respectively. The sphere is coloured blue, and a cutaway of the tube is provided to reveal the relevant isosurfaces.

It was hypothesized that a similar bifurcation scenario will occur in this system, with non-axisymmetric flow predicted to emerge prior to the axisymmetric Hopf bifurcation. A series of three-dimensional computations were performed over a range of Reynolds numbers below the predicted axisymmetric transition point to test identify any non-axisymmetric flow regimes. In the range  $355 < Re < 360$ , the axisymmetric wake was found to transition to a non-axisymmetric state, producing a steady non-axisymmetric flow. This implies that the first-occurring non-axisymmetric transition occurs through a regular bifurcation. At slightly higher Reynolds numbers, the steady non-axisymmetric wake underwent a subsequent transition to unsteady flow. This second transition occurs in the range  $360 < Re < 365$ .

The steady and unsteady non-axisymmetric wakes differed little in structure – the unsteady flow tended to manifest itself as a low-frequency pulsing in the flow, rather than adopting the hairpin shedding observed behind free spheres (Magarvey & MacLatchy, 1965; Johnson & Patel, 1999).

An isosurface plot of the saturated steady non-axisymmetric solution at  $Re = 360$  is shown in figure 10. In this plot, the pressure gradient decreases from the top right to the bottom left of the tube section displayed, and relative to the sphere, the tube wall is moving from the bottom left to the top right. A useful comparison between the steady non-axisymmetric wake behind a sphere in open flow (Thompson *et al.*, 2001) and the non-axisymmetric flow shown here can be made. Both are characterised by a counter-rotating pair of streamwise vortices, which for a free sphere extend far downstream, but in this case the downstream presence of the next sphere disrupts the flow and dissipates the vortices. Notably, this non-axisymmetric flow has a net side force associated with it, similar to a sphere in open flow. Thus in the applications where the spheres represent particles or bodies free to move through the tube, this state would cause the spheres to migrate away from the centreline, dramatically changing the flow.

## CONCLUSION

A numerical study employing axisymmetric and three-dimensional spectral-element computations has investigated the pressure-driven flow past an array of equi-spaced spheres positioned axisymmetrically in a circular tube. For a fixed diameter and spacing ratio,  $SR = 1.0$  and  $DR = 0.6$ , critical Reynolds numbers at which the zero-net-flow and zero-net-drag conditions occurred were found to be  $Re \approx 111.5$  and  $Re \approx 26.5$ , respectively. In addition, linear collapses to the relative flow rate data and the product of axial force on each sphere and Reynolds number were established when plotted against the product of Reynolds number and axial pressure gradient. Strong linearity was found at  $Re \, dP/dz < 1500$  for  $Q_{rel}$ , and up to  $Re \, dP/dz \approx 12000$  for  $Re \, F_D$ .

Contour plots of vorticity were shown to demonstrate that changes in diameter ratio dramatically altered the flow surrounding the sphere, whereas for changes in the sphere spacing, the effect was barely noticeable. Finally, a three-dimensional iso-surface plot of non-axisymmetric streamwise vortical structures in the flow local to a single repeating tube unit was shown to verify that the axisymmetric solution transitioned to a steady non-axisymmetric flow prior to undergoing an unsteady bifurcation of the axisymmetric flow. Importantly, non-axisymmetry developed at a Reynolds number far in excess of the Reynolds numbers experienced by particles free to migrate along the centreline, based on the zero-net-drag condition identified in this study.

## ACKNOWLEDGEMENTS

The authors wish to thank the Australian Partnership for Advanced Computing (APAC) for providing access to the computing facilities required to complete this study through the merit allocation scheme. G.J.S. and K.R. received salary through Australian Postdoctoral Fellowships on ARC Discovery Grants DP0555897 and DP0665736, respectively.

## REFERENCES

- BLACKBURN, H.M. and SHERWIN, S.J., (2004), "Formulation of a Galerkin spectral element–Fourier method for three-dimensional incompressible flows in cylindrical geometries", *J. Comp. Phys.*, 197, 759-778.
- Fitz-Gerald, J.M., (1969), "Mechanics of red-cell motion through very narrow capillaries", *Proc. Roy. Soc. Lond. B.*, 174, 193-227.
- GHIDERSA, B. and DUŠEK, J., (2000), "Breaking of axisymmetry and onset of unsteadiness in the wake of a sphere", *J. Fluid Mech.*, 423, 33-69.
- JOHNSON, T.A. and PATEL, V.C., (1999), "Flow past a sphere up to a Reynolds number of 300", *J. Fluid Mech.*, 378, 19-70.
- KARNIADAKIS, G.EM., ISRAELI, M. and ORSZAG, S.A., (1991), "High-order splitting methods for incompressible Navier-Stokes equations", *J. Comp. Phys.*, 97, 414-443.
- KARNIADAKIS, G.EM. and SHERWIN, S.J., (2005), "Spectral/hp element methods for computational fluid dynamics", *Oxford University Press*.
- LIGHTHILL, M.J., (1968), "Pressure-forcing of tightly fitting pellets along fluid-filled elastic tubes", *J. Fluid Mech.*, 34, 113-143.
- MAGARVEY, R.H. and MACLATCHY, C.S., (1965), "Vortices in sphere wakes", *Canadian J. Phys.*, 43, 1649-1656.
- ORTEGA, J.M., BRISTOL, R.L. and SAVAS, O., (1998), "Flow resistance and drag forces due to multiple adherent leukocytes in postcapillary vessels", *Biophys. J.*, 74, 3292-3301.
- POZRIKIDIS, C., (2005), "Numerical simulation of cell motion in tube flow", *Annals of Biomed. Eng.*, 33(2), 165-178.
- SECOMB, T.W., HSU, R. and PRIES, A.R., (1998), "A model for red blood cell motion in glycocalyx-lined capillaries", *Am. J. Physiol. Heart Circ. Physiol.*, 274, 1016-1022.
- SECOMB, T.W., HSU, R. and PRIES, A.R., (2001), "Motion of red blood cells in a capillary with an endothelial surface layer: Effect of flow velocity", *Am. J. Physiol. Heart Circ. Physiol.*, 281, 629-636.
- SHEARD, G.J., THOMPSON, M.C. and HOURIGAN, K., (2003), "From spheres to circular cylinders: Stability and flow structures of bluff ring wakes", *J. Fluid Mech.*, 492, 147-180.
- SMYTHE, W.R., (1961), "Flow around a sphere in a circular tube", *Phys. Fluids*, 4(6), 756-759.
- SMYTHE, W.R., (1964), "Flow around a spheroid in a circular tube", *Phys. Fluids*, 7(5), 633-638.
- THOMPSON, M.C., LEWEKE, T. and PROVANSAL, M., (2001), "Kinematics and dynamics of sphere wake transition", *J. Fluid Struct.*, 15, 575-585.
- TÖZEREN, H., (1983), "Drag on eccentrically positioned spheres translating and rotating in tubes", *J. Fluid Mech.*, 129, 77-90.
- TÖZEREN, H. and SKALAK, R., (1978), "The steady flow of closely fitting incompressible elastic spheres in a tube", *J. Fluid Mech.*, 87, 1-16.
- TÖZEREN, H. and SKALAK, R., (1979), "Flow of elastic compressible spheres in tubes", *J. Fluid Mech.*, 95, 743-760.
- WANG, W. and PARKER, K.H., (1998), "Movement of spherical particles in capillaries using a boundary singularity method", *J. Biomech.*, 31, 347-354.